Ag2Se Nanowire Network as an Effective In-Materio Reservoir Computing Device

Takumi Kotooka
Kyushu Institute of Technology
Sam Lilak
University of California Los Angeles
Adam Stieg
University of California Los Angeles https://orcid.org/0000-0001-7312-9364
James Gimzewski
University of California Los Angeles https://orcid.org/0000-0003-4333-6957
Naoyuki Sugiyama
National Institute for Materials Science
Yuichiro Tanaka
Kyushu Institute of Technology
Hakaru Tamukoh
Kyushu Institute of Technology
Yuki Usami
Kyushu Institute of Technology
Hirofumi Tanaka (tanaka@brain.kyutech.ac.jp)
Kyushu Institute of Technology https://orcid.org/0000-0002-4378-5747

Article

Keywords: Artificial Intelligence, Nonlinear Nanojunctions, Higher Harmonic Generation, Waveform Generation Tasks, Voice Classification

Posted Date: March 17th, 2021

DOI: https://doi.org/10.21203/rs.3.rs-322405/v1

Ag_2Se Nanowire Network as an Effective In-Materio Reservoir Computing Device

*Takumi Kotooka, Sam Lilak, Adam Z. Stieg, James K. Gimzewski, Naoyuki Sugiyama, Yuichiro Tanaka, Hakaru Tamukoh, Yuki Usami and Hirofumi Tanaka**

T. Kotooka, Y. Tanaka, H. Tamukoh, Y. Usami, H. Tanaka
Department of Human Intelligence Systems, Graduate School of Life Science and Systems Engineering, Kyushu Institute of Technology (Kyutech), Kitakyushu 808-0196, Japan.

S. Lilak, J. K. Gimzewski
Department of Chemistry and Biochemistry, University of California Los Angeles (UCLA), Los Angeles, CA 90095, U.S.A.

A. Z. Stieg, J. K. Gimzewski
California NanoSystems Institute, University of California Los Angeles (UCLA), Los Angeles, CA 90095, U.S.A.

A. Z. Stieg, J. K. Gimzewski, WPI Center for Materials Nanoarchitectonics (MANA), National Institute for Materials Science (NIMS), Tsukuba 305-0044, Japan.

Y. Tanaka
Japan Society for Promotion of Science, Tokyo 1020083, Japan

J. K. Gimzewski, H. Tamukoh, Y. Usami, H. Tanaka
Research Center for Neuromorphic AI Hardware, Kyutech, Kitakyushu 8080196, Japan.

N. Sugiyama
Transmission Electron Microscopy Station, National Institute for Materials Science (NIMS), Tsukuba, Ibaraki, 3050044, Japan.

N. Sugiyama
Toray Research Center Inc. Morphological Research Laboratory 3-3-7 Sonoyama, Otsu, Japan

*Corresponding author: tanaka@brain.kyutech.ac.jp

Abstract

Modern applications of artificial intelligence (AI) are generally algorithmic in nature and implemented using either general-purpose or application-specific hardware systems that have high power requirements. In the present study, physical (in-materio) reservoir computing (RC) implemented in hardware was explored as an alternative to software-based AI. The device, made up of a random, highly interconnected network of nonlinear Ag_2Se nanojunctions, demonstrated the requisite characteristics of an in-materio reservoir, including but not limited to nonlinear switching, memory, and higher harmonic generation. As a hardware reservoir, the devices successfully performed waveform generation tasks, where tasks conducted at elevated network temperatures were found to be more stable than those conducted at room temperature. Finally, a comparison of voice classification, with and without the network device, showed that classification performance increased in the presence of the network device.

Introduction

Artificial intelligence (AI) technology has become a very important research topic and has attracted considerable attention. However, most current AI systems rely solely on purpose-built software for their application. For the software to recognize and detect the status of large amounts of unstructured data, significant power is required for computer processing. Research in this field aims to reduce traditional AI software systems' power consumption by by performing these complex learning tasks in-situ.

Recently, several hardware AI implementations have been suggested for ANNs.[1–4] Our previous work demonstrated reservoir computing (RC), in a recurrent neural network (RNN),[5–7] as a suitable candidate to replace the AI software system with a random network of nonlinear nanojunctions.[8] Thus, we focused on RC hardware for in-materio computing, which is expected to operate with a significantly lower power consumption than traditional AI software.[9] RC classification only requires weighting of a single layer of output signals from

the RNN, which is efficient compared to other ANN systems (Fig. 1). Compared to other neural networks, the random network does not require a detailed device design, enabling the intrinsic properties of the physical system to be directly utilized for computation in-materio.[10] Theoretical results have shown in-materio RC to be capable of voice classification.[11] To date, most studies of in-materio RC[12–15] have only involved simulations or performance of simple tasks, while actual practical implementations have not been demonstrated. Atomic switch networks (ASNs) - highly-interconnected nanowire networks comprising memristive inter-wire junctions - are strong candidates for in-materio RC, where device nonlinearity results from the low potential of the redox reaction occurring at the nanowire junctions during voltage-induced switching.[16–18] To date, the implementation of an RC system via an ASN has been achieved primarily using Ag_2S.[19] However, Ag_2S is easily decomposed by Joule heating, thereby limiting long-term stability. To improve device stability, the development of alternative materials to be used in the ASN device architecture for application to in-materio RC is explored.

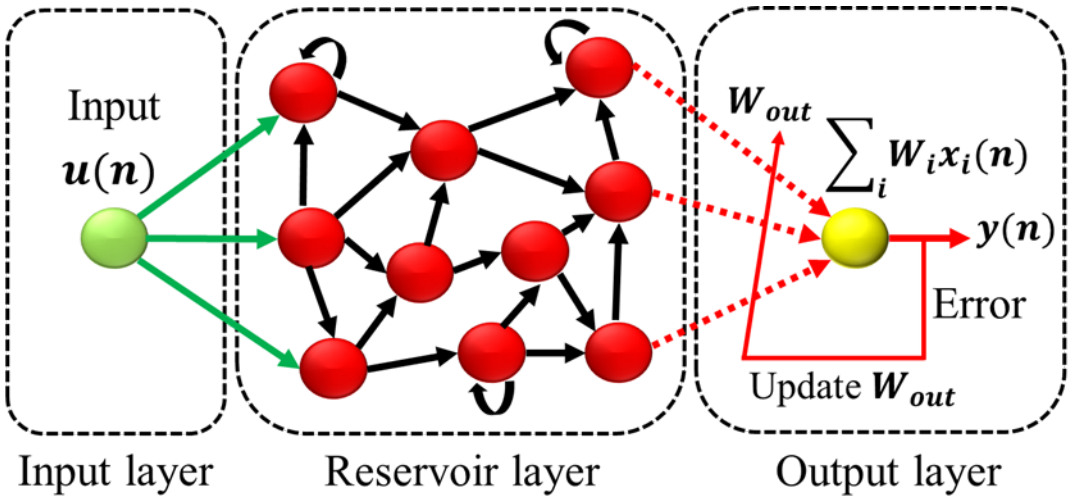

Figure 1| Reservoir computing (RC). An RC system is composed of three layers: input, reservoir, and output. The calculated wavefunction is a linear combination of output signals, weighted through learning to ensure the best approximation to a target waveform, $y(n)$.

We investigated the use of β-Ag_2Se[20] as a material substrate for in-materio RC. β-Ag_2Se has a stable crystal structure below 408 K, is a narrow-bandgap semiconductor, and is thermoelectric owing to its high electrical conductivity, low lattice thermal conductivity, and high Seebeck coefficients.[21] β-Ag_2Se (herein referred to as Ag_2Se) has electrical switching characteristics similar to the more well-characterized Ag_2S resulting from the surface redox reaction of Ag ions[22] and has desirable properties in terms of high thermal durability. Moreover, the reported synthesis methods for Ag_2Se nanowires are both straightforward and cost-effective for scalable device fabrication.[23–25]

ASN devices for RC were fabricated from Ag_2Se nanowires and their operational properties were evaluated. The Ag_2Se-ASN device displayed nonlinear switching and memory properties owing to the atomic switch junctions embedded in the ASN. In addition, the power spectral density (PSD) displayed a higher level of harmonic generation, indicating high network dimensionality. Performance of benchmark RC tasks demonstrated the ability of the random network to efficiently process and learn time-series data. Here, the voice classification performance improved when the ASN was introduced into the task.

Ag_2Se Nanowire Characterization

The as-synthesized Ag_2Se nanowires and the network morphology were characterized by SEM, as shown in Fig. 2(a), Fig. S1(c), and (d), and confirmed not to be altered from the original Se nanowire template. Characteristic peaks associated with Ag_2Se could be clearly identified in the XRD spectrum shown in Fig. 2(b), confirming the formation of Ag_2Se nanowires. The rough surface of the Ag_2Se nanowires, as revealed by STEM and shown in Fig. 2(c), suggests that nanowires grow via clustering of the nanoparticles, as previously reported for Se nanowire growth.[26] Electron beam diffraction confirmed the material to be a single crystal, as shown in the inset of Fig. 2(c) with a lattice spacing of 0.25 nm. The selected area electron diffraction

(SAED) pattern shown in Fig. 2(d) indicates that the distributions of Ag and Se in the Ag_2Se nanowire were almost identical, and no significant segregation was observed.

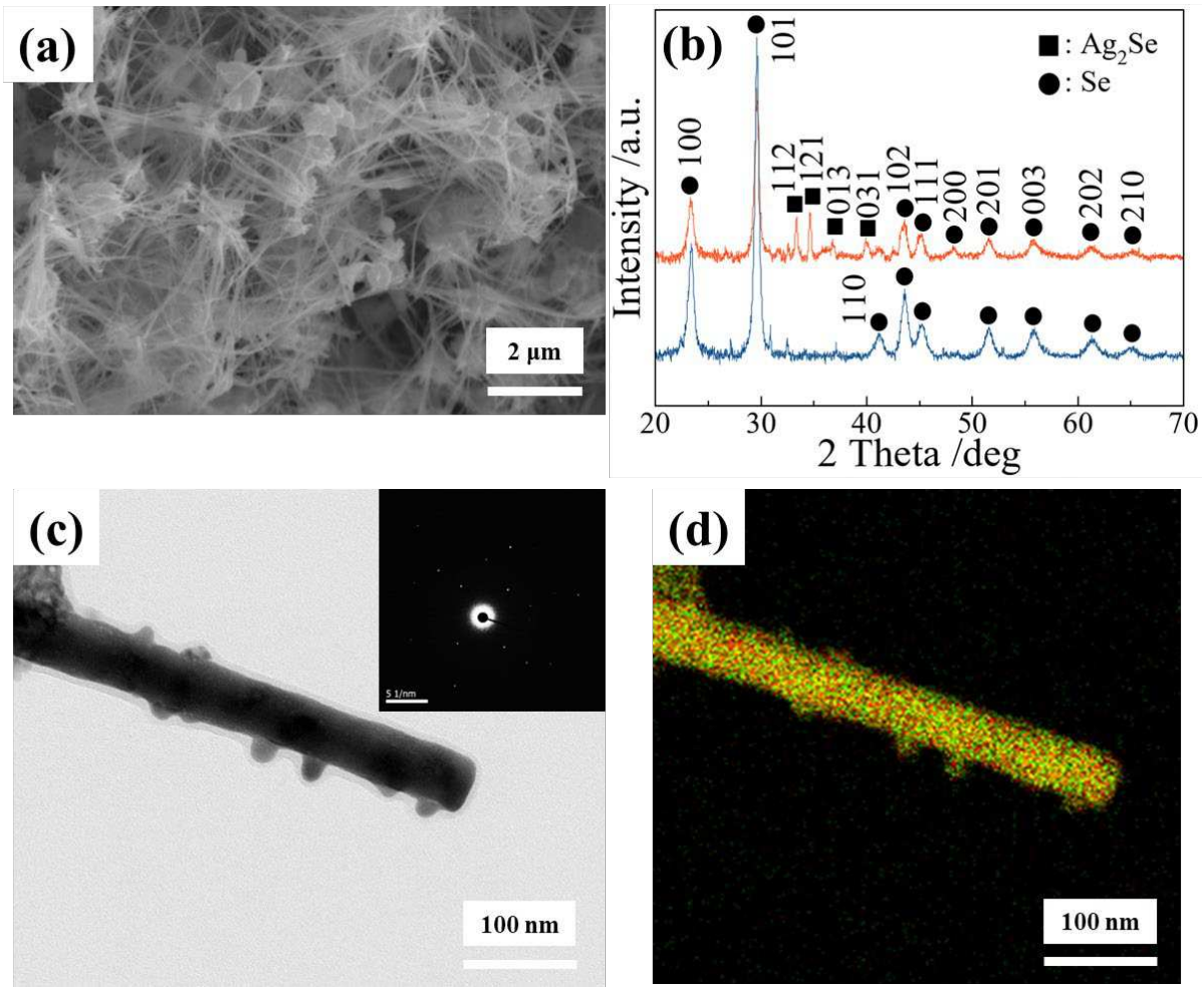

Figure 2| Structural characterization of Ag_2Se. a, SEM image and **b,** XRD results of synthesized Ag_2Se nanowires after submerging in a $AgNO_3$ solution. The blue and orange curves represent the nanowires before and after reaction in the $AgNO_3$ solution, respectively. **c,** STEM image of synthesized Ag_2Se nanowire. Inset: SAED pattern of Ag_2Se indicating single crystallinity. **d,** EDS results showing stoichiometric distribution of Ag and Se in the Ag_2Se nanowire. Red and green dots indicate the positions of Ag and Se, respectively.

Electrical Properties of Ag_2Se-ASN Devices

Generally, volatile memory, nonlinear dynamics, and the ability to handle high-dimensional data (high dimensionality) is required for implementation of in-materio RC. In addition, electrical properties such as phase shifts and higher harmonic generation (HHG) are necessary for a variety of outputs.

Electrical characterization in the form of *V*–*t* curves shown in Fig. 3(a) was carried out by delivering an 11 Hz, 1 V sine wave to fabricated devices as shown in Fig. S1(a). The electrode position labeled 1 was selected as input and orthogonal electrodes positioned at 5, 12, and 16 were used as outputs. The resulting output displayed phase shifts between the input and output signals, indicating the presence of capacitive and inductive properties in addition to memory elements within the Ag_2Se nanowire network. Figure 3(b) shows a PSD plot obtained from the *V*–*t* curve via fast Fourier transform (FFT) analysis. Peaks appeared not only at 11 but also at 22 and 33 Hz, indicating higher harmonics generation (HHG), which is a high-dimensional property arising from interactions amongst the complex, interconnected network of nonlinear junctions.

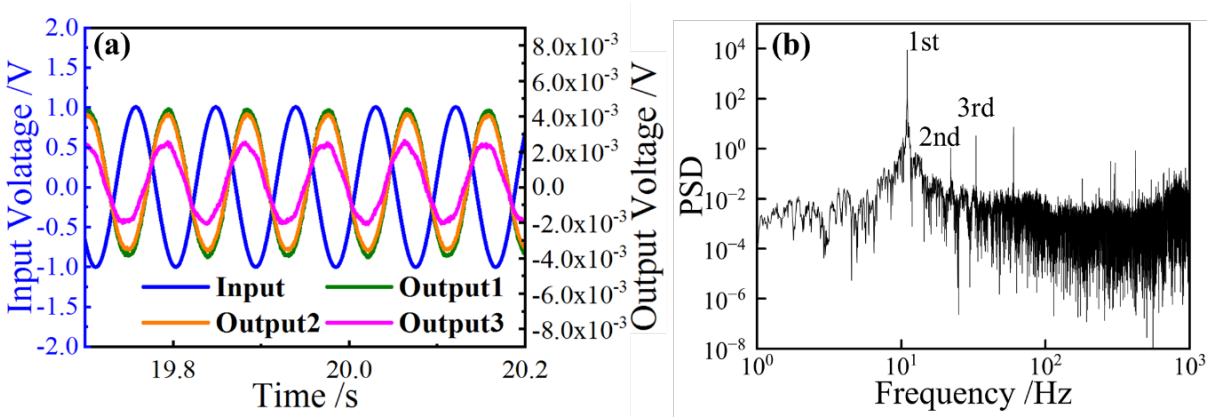

Figure 3| Electronic properties of Ag_2Se nanowire device.

a, *V-t* curves and **b,** PSD diagram for a device responding to an input signal. Four probes were used for the *V-t* measurements where the input signal was a sinusoidal voltage (amplitude: ± 1 V, frequency: 11 Hz) and there were three output signals. The blue curve

represents the input signal. The output signals were obtained from a random network device made from Ag_2Se nanowires.

Lissajous plots of the ASN reveals the dynamic responses intrinsic to the system and can capture the changes in the network when inherent nonlinear responses such as switching behavior occur.[27]

The shape of these curves reveals both linear and nonlinear relationships. Mathematically, the relationship between the output and the periodic input produces curves can be represented by the following equations:

$$x(t) = Asin(\omega t) \text{ and} \quad (2)$$

$$y(t) = \sum_{i=0} A_i sin(\omega_i t - \delta_i), \quad (3)$$

Where A and ω are the input amplitude and frequency, respectively. A_i, ω_i, and δ_i are the output amplitudes, frequencies, and phase delays, respectively.

The operational dynamics of an Ag_2Se-ASN is expected to be temperature dependent, and thus is expected to affect the RC functionality. Lissajous curves (*V*-*V*) were used to determine the temperature dependence of the electrical properties of the Ag_2Se nanowire device[27] based on the input and output behavior of continuous systems. Figure S2 shows the Lissajous curves obtained at 15, 300, and 343 K. At 15 K, the shape of the curve is angular, with no elliptical shape being observed, implying that atomic switching occurred in the network and there was no phase shift. The shape was elliptical at 300 K, indicating that weak switching with presence of dominant capacitance was occurred, and that phase shift had happened. This non-dominant switching behavior would be generated from collective properties of surface redox dynamics interconnecting junctions. This dynamical behavior is suitable for RC applications because condition inside reservoir should not change in reservoir system. The Lissajous curves at 343 K displayed angular and elliptical regions, indicative of both a phase shift and atomic switching behavior. As the temperature rises, the junctions in the network become unstable, as does the

output; at 343 K, it is assumed that the process of the junctions being broken by heat and then re-forming as a result of the application of a voltage is repeated.

Benchmark Tasks for RC

To investigate the task performance of the Ag_2Se-ASN as a RC device, two tasks were conducted (waveform generation and voice classification). The waveform generation task requires a nonlinear transformation of time-varying inputs for the signals, a voice classification task must be able to sufficiently process time-series data.

We performed waveform generation tasks to verify the performance of the Ag_2Se-ASN as an in-materio reservoir. Several specific waveforms (cosine, triangle, sawtooth, square) were learned by performing ridge regression[28] on the output layer of the device, with the nanowire network serving as the reservoir layer, as shown in Figure 6a. These results were evaluated by calculating the normalized mean-square error (NMSE) and accuracy, as follows:

$$NMSE(x, y) = \frac{\sum_i (x_i - y_i)^2}{\sum_i (x_i)^2} \quad (4)$$

$$\text{Accuracy}(x, y) = 1 - \frac{\sum_i (x_i - y_i)^2}{\sum_i (x_i - \bar{x})^2} \quad (5)$$

Where, x, $\bar{x}$, and y are the output data, mean of outputs, and target data respectively. Figure 4(b) shows the results of the waveform generation task, where the red and blue plots represent the target and generated waveforms, respectively. The NMSEs of the cosine and triangle waveform generation were markedly smaller than those of the other waveforms, which can be attributed to the relative difficulty of the task. The accuracy of the cosine and triangle waveforms were nearly 99%, which exceeds previously reported task performance using Ag_2S nanowire networks,[19] even though fewer output electrodes were used. The generation of waveforms having a similar frequency and line shape as the input signal is expected to be relatively simple, as opposed to waveforms having higher-frequency components. The accuracy of the task for sawtooth and square waveforms was therefore lower, with larger associated NMSE values.

To perform higher-precision waveform learning, a more complex network is required to obtain the different outputs. Learning depends on the outputs from the device functioning as a reservoir, which is believed to improve the higher dimensional and nonlinear properties. Figure 4(c) shows the accuracy of a waveform generation task at different temperatures. The waveform generation results obtained at high temperatures are shown in the Supplementary Information (Figs. S3, S4, and S5), and the NMSE results are shown in Fig. 4(d). The accuracy decreased with an increase in the temperature except in the case of the sawtooth waveform, although it did not perform significantly worse. This indicates that the Ag_2Se device was relatively stable at high temperatures. The accuracy of learning at 343 K was highest for the sawtooth waveform task, because the shape of the output signal at 343 K is a result of the superimposition of many harmonics. Figures S6, S7, and S8 indicate the HHGs that appeared at higher temperatures than at 300 K. Referring to the results of the Lissajous plot, the waveform generation task required a phase shift and did not display switching behavior. The task results above 300 K were also relatively consistent with the target waveform.

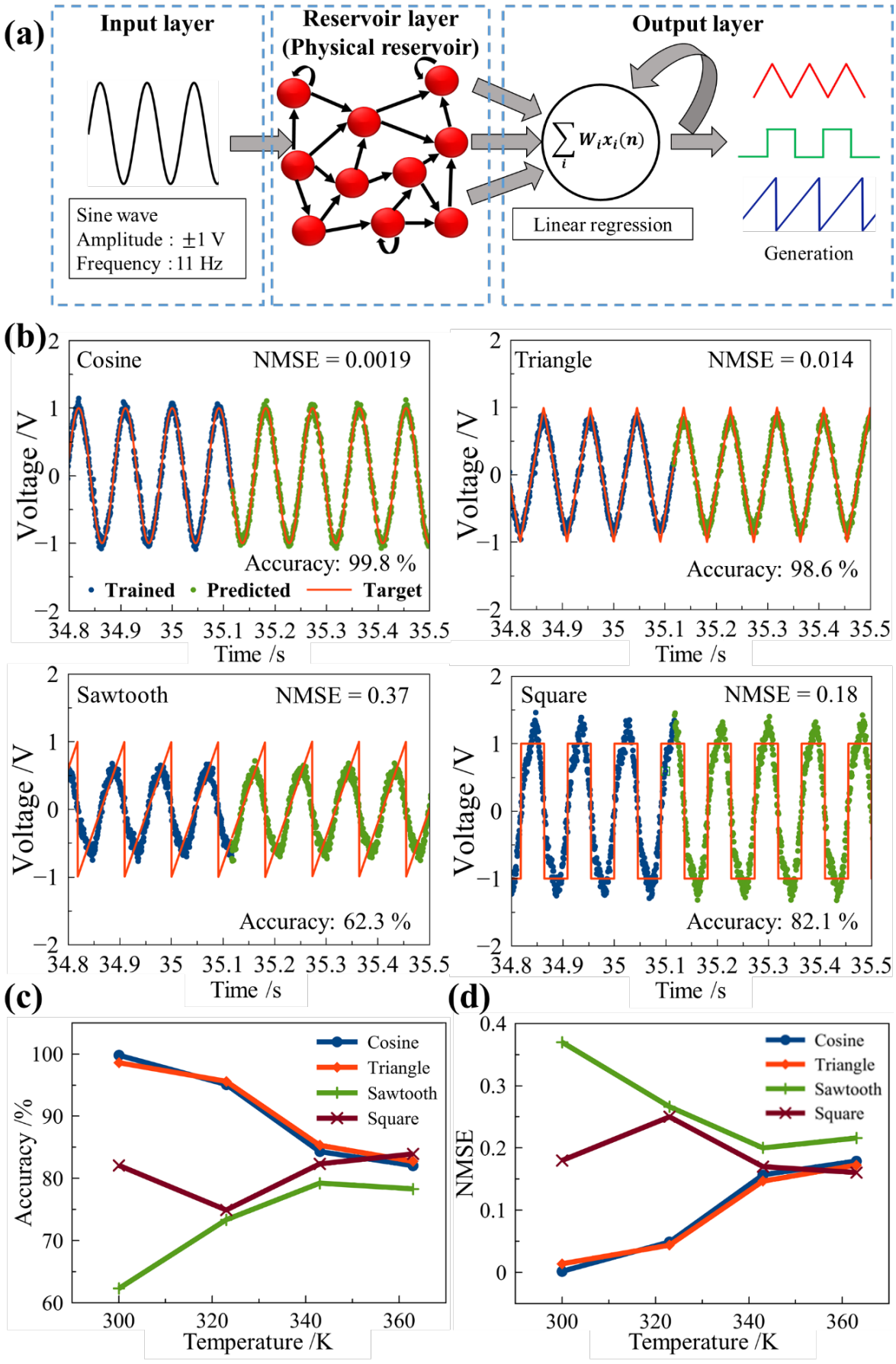
(a)
Input layer
Reservoir layer
(Physical reservoir)
Output layer
Sine wave
Amplitude : ±1 V
Frequency : 11 Hz
$\sum_i W_i x_i(n)$
Linear regression
Generation
(b)
Cosine
NMSE = 0.0019
Accuracy: 99.8 %
Trained
Predicted
Target
Triangle
NMSE = 0.014
Accuracy: 98.6 %
Sawtooth
NMSE = 0.37
Accuracy: 62.3 %
Square
NMSE = 0.18
Accuracy: 82.1 %
Voltage /V
Time /s
(c)
Accuracy /%
Temperature /K
(d)
NMSE
Temperature /K
Cosine
Triangle
Sawtooth
Square

Figure 4| Results of waveform generation task. a, Procedure for waveform-generation task. The input was a sinusoidal wave (amplitude: ± 1 V, frequency: 11 Hz) in air. **b,** Results of waveform generation tasks at room temperature. Target waves were cosine, triangle, sawtooth, and square waves shown at top left, top right, bottom left, and bottom right, respectively. NMSE is an abbreviation for "normalized mean square error." **c**,**d,** Accuracy and NMSE of specific tasks at different temperatures, respectively.

Voice classification is a crucial task in numerous AI applications, where the capacity to identify and classify a diverse range of spoken digits is paramount. In the RC context, voice classification requires that the reservoir operate as a nonlinear transformer of input data. A voice classification task was performed shown in Fig. 5(a). Using the free-spoken digit data (FSDD) as shown in Fig. 5(a). This dataset consisted of ten numbers from zero to nine pronounced by six different speakers.[29] For each number, the recorded data was for fifty readings.

Table 1 lists the calculated scores: accuracy, recall, precision, and F1 scores.[30] The scores were calculated using the following equations:

$$Accuracy = \frac{TP + TN}{TP + FP + FN + TN} \tag{6}$$

$$Recall = \frac{TP}{TP + FN} \tag{7}$$

$$Precision = \frac{TP}{TP + FP} \tag{8}$$

$$F1\ score = 2 \times \frac{precision \times recall}{precision + recall} \tag{9}$$

where TP, FN, FP, and TN indicate the number of true positive, false negative, false positive, and true negative results, respectively.

Table 1. Confusion Matrix

	Predicted Positive	Predicted Negative
Actual Positive	True Positive (TP)	False Negative (FP)
Actual Negative	False Positive (FP)	True Negative (TN)

The results of voice classification obtained with and without the Ag_2Se reservoir device are shown in Fig. 5. The confusion matrix obtained by SVM of the ten numbers from 0 to 9 spoken by Jackson with and without the device are shown in Fig. 5(b) and 5(c), and that of "zero" spoken by the four persons with and without the device are shown in Fig. 5(d) and 5(e) respectively. Generally, the classification performance is considered accurate if the diagonal values in the confusion matrix are large closing in on one. By comparing the matrices obtained with and without the Ag_2Se reservoir devices, the performance with the Ag_2Se reservoir device for the classification of 10 numbers (shown in Fig. 5(c)), and the classification of four speakers (shown in Fig. 5(e)), were higher than that without the Ag_2Se reservoir device (Fig. 5(b) and 5(d), respectively). The classification scores of both tasks with the Ag_2Se reservoir device also became higher than without the device (Fig. 5(f) and 5(g), respectively). Figure S9 shows the voice classification results at different temperatures (323, 343, and 363 K) and the performance of classification results was not change, which indicated the Ag_2Se device has thermal stability from this task. These results indicate that the classification performance improved more when the Ag_2Se reservoir device was used as the input to SVM. The poor performance without the Ag_2Se reservoir device was believed to be due to the lack of the nonlinear property, which affects the mapping of the data to a classification space. The high-dimensional property of the Ag_2Se reservoir device may facilitate the classification task by mapping the input data to a high-dimensional space. The obtained results indicate that the Ag_2Se reservoir device can act as a nonlinear transformer and used for classification and possibly more complex tasks.

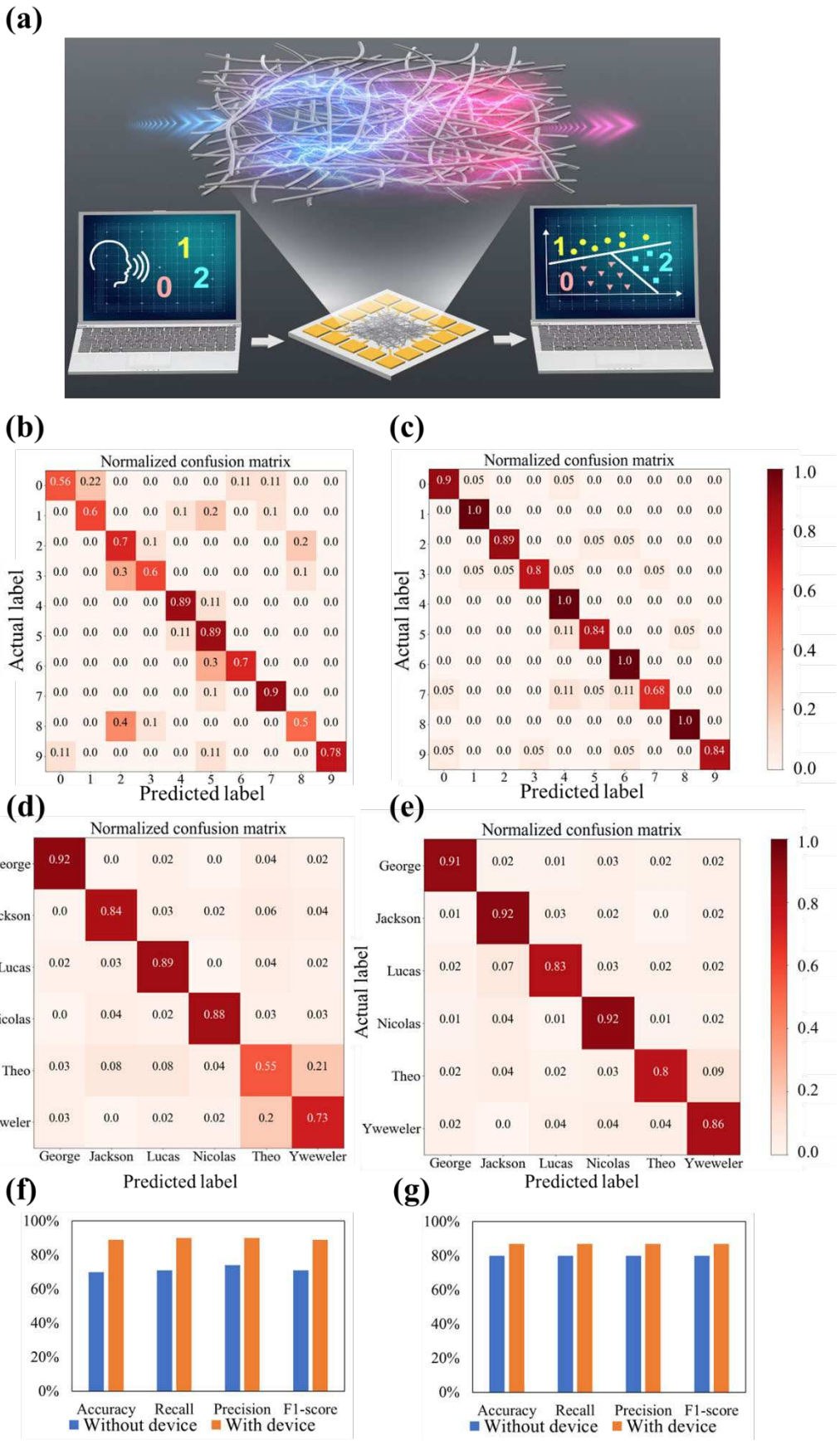
(a)
1
0
2
1
0
2
(b)
Normalized confusion matrix
Actual label
Predicted label
(c)
Normalized confusion matrix
Actual label
Predicted label
(d)
Normalized confusion matrix
George
Jackson
Lucas
Nicolas
Theo
Yweweler
Actual label
Predicted label
(e)
Normalized confusion matrix
George
Jackson
Lucas
Nicolas
Theo
Yweweler
Actual label
Predicted label
(f)
100%
80%
60%
40%
20%
0%
Accuracy
Recall
Precision
F1-score
Without device
With device
(g)
100%
80%
60%
40%
20%
0%
Accuracy
Recall
Precision
F1-score
Without device
With device

Figure 5| Classification results for ten numbers and six speakers. a, Schamatic of voice classification procedure. FSDD was utilized as the voice dataset. Six speakers (George, Jackson, Nicolas, Theo, Yweweler, and Lucas) and ten numbers from zero to nine were classified. The voice data was subjected to FFT preprocessing and was fed into to the Ag_2Se device as an analog signal. There was one input and two outputs, and the input was an analog-converted signal from 0 to 9. Outputs were labeled and used for model construction and the determination of test performance. Confusion matrices **b,** without and **c,** with the Ag_2Se reservoir device of classifying ten numbers from zero to nine spoken by Jackson, respectively. **d**,**e,** Confusion matrices classifying six speakers **d** without and **e** with the Ag_2Se reservoir device. **f**,**g,** Classification scores with and without the Ag_2Se reservoir device for **f** ten numbers and **g** six speakers.

Conclusion

We fabricated a material-based in-materio reservoir device comprised of a Ag/Ag_2Se nanowire random network which had all the requisite properties for use in RC, such as nonlinearity, phase shift, and HHG. The Ag_2Se nanowire random network device exhibited switching behavior at 15 K, but not above room temperature in which redox dynamics at Ag_2Se nanowire's junctions is generated. Specific waveforms were generated from the sinusoidal input signal via a waveform learning task performed by the RC device. The results indicate that the device can recognize time-series data such as voice classification. The Ag_2Se nanowire device was significantly more stable when performing RC tasks between 300 and 363 K than Ag_2S nanowires. The Ag_2Se nanowire random network device improved voice classification performance as a nonlinear transformer, and it is expected to be successful at more complex

time-series classification tasks, potentially achieved by adaptive and dynamical system arising from the topology in-materio.

Methods

Synthesis of Ag_2Se Nanowires

The synthesis method was previously described in Ref. 23. Sodium selenite (0.25 g, Sigma Aldrich 99.9%) and glucose (1.5 g, Wako, 98%) were added to 100 ml deionized (DI) water at 363 K without stirring. After 20 min, the solution was quenched, and a brick-red precipitate of α-Se settled to the bottom of a flask. The precipitate was rinsed with DI water and then dispersed in isopropanol and sonicated for 5 min. After sonication, the suspension was stored in the dark at T ~ 295 K for one week to allow t-Se nanowires to form from the α-Se. The suspension was then centrifuged (4000 rpm, 5 min) and the supernatant removed. To obtain Ag_2Se nanowires, the t-Se nanowires were redispersed in an $AgNO_3$ solution (50 mM) for 3 h. Ag_2Se nanowires were synthesized according to Equation (1) below. Finally, the product was rinsed with DI water at 363 K to remove impurities, thus yielding pure Ag_2Se nanowires.

$$3Se_{(s)} + 6Ag^{+}_{(aq)} + 3H_2O \rightarrow 2Ag_2Se_{(s)} + Ag_2SeO_{3(s)} + 6H^{+}_{(aq)} \quad (1)$$

The synthesized product was characterized by X-ray diffraction (XRD), scanning electron microscopy (SEM), scanning transmission electron microscopy (STEM), and energy-dispersive X-ray spectroscopy (EDS) to verify the morphology, crystallinity and chemical composition.

Device Fabrication and Electrical Measurements

The fabrication procedure of the random Ag_2Se nanowire network device is shown in Fig. S1. An aluminum electrode pattern (Fig. S1(a)) was fabricated on a thermally oxidized (200 nm) Si wafer using e-beam (electron-beam) lithography using the ELIONOX ELS-7500. The resist for e-beam lithography (gL 2000: anisole = 1:1, Gluon Lab) was spin-coated onto the SiO_2 substrate (5000 rpm, 40 s) and subsequently baked at 453 K for 2 min. The resist-coated SiO_2

substrate was exposed to an electron beam (amplitude 30 nA) and developed in a ZED-N50 (Zeon) solution for 5 min. After development, Al sputtering was employed to deposit electrodes (60 nm). A magnified image of the center of the device is shown in Fig. S1(b). Finally, the patterned electrodes were submerged in a dimethyl sulfoxide solution at 353 K for 20 min so that they lifted-off. The random Ag_2Se nanowire network was then fabricated by drop-casting the Ag_2Se solution in the center of the electrode array and these electrodes were labeled at each position as shown in Fig. S1(c). The formation of the Ag_2Se nanowire network was confirmed by SEM, as shown in Fig. S1(d).

The *V*-*t* (voltage-time) characteristics were measured using a function generator (HEWLETT PACKARD model 33120A) and a DAQ System (National Instruments model 9234) controlled by software coded using LabVIEW. The low-temperature *V*–*t* characteristics were measured using a low-temperature probe system (PLF-101-4, Pascal Co., Ltd.). A silicon rubber heater provided heating for high-temperature measurements (up to 363 K). The position 1 electrode was selected as the input, while the others were used as outputs.

Voice Classification Task

The FSDD was used as a dataset for voice classification and consisted of ten numbers from zero to nine pronounced by six different speakers.[29] Each number contains recorded data that has been pronounced 50 times. In this experiment, we used six speakers (George, Jackson, Nicolas, Theo, Yweweler, and Lucas) and the recorded data of zero to nine pronounced 50 times. The conversion of the raw data by FFT was the first step in the procedure. An analog signal was input to the Ag_2Se reservoir device as time-series data by converting the frequency value of an FFT datapoint to the corresponding time value with Labview systems. In a single input, each frequency component of the spectrogram of a single pronounced number was input in turn. One electrode was used as the input and two as the outputs, and the sampling rate in the measurement was 1000 step/s. The labeling for classification and training of the classifier was

conducted in python. The measured data from device was labeled for classification and divided into groups for training and predicting tasks in the ratio 80:20. The linear combination of output signals was used for the classification task. A support vector machine (SVM) was used as a classifier in the learning step.[31] To adjust the hyperparameters (C and gamma) of the SVM system, k-fold cross-validation was applied.[32] Two different classification tasks were performed, namely the classification of different speakers and the classification of pronounced numbers. In this experiment, we compared the difference in classification results between the case with and without the device. In the case of without the device, the FFT processed data was labeled and input to the classifier for classification.

Supporting Information
Supporting Information is available from the Wiley Online Library or from the author.

Acknowledgements

T.K. sincerely appreciates the financial support from the Japanese Society for the Promotion of Science (JSPS) under the Tobitate JAPAN Program, allowing him to stay at UCLA for seven months. Part of this work was financially supported by KAKENHI (grant nos. 19H02559, 19K22114, and 20K21819) and was conducted at the Kitakyushu Semiconductor Center, supported by the Nanotechnology Platform Program (Nanofabrication) of the Ministry of Education, Culture, Sports, Science, and Technology (MEXT), Japan.

Received: ((will be filled in by the editorial staff))
Revised: ((will be filled in by the editorial staff))
Published online: ((will be filled in by the editorial staff))

References

[1] Esser, S. K., et al. Convolutional networks for fast, energy-efficient neuromorphic computing. *Proc. Natl. Acad. Sci. USA* **113(41)**, 11441-11446 (2016).

[2] Wen, W., et al. A new learning method for inference accuracy, core occupation, and performance co-optimization on TrueNorth chip. In *2016 53nd ACM/EDAC/IEEE Design Automation Conference (DAC)* (pp. 1-6). IEEE (2016).

[3] Davies, M. et al. Loihi: A Neuromorphic Manycore Processor with On-Chip Learning. *IEEE Micro* **38(1)**, 82 (2018).

[4] Michaelis, C., Lehr, A. B., Tetzlaff, C. Robust Trajectory Generation for Robotics Control on the Neuromorphic Research Chip Loihi. *Front. Neurorobot*. **14**, 11 (2020).

[5] Jaeger, H., & Haas, H. Harnessing nonlinearity: Predicting chaotic systems and saving energy in wireless communication. *Science* **304(5667)**, 78-80 (2004).

[6] Lukoševičius, M., & Jaeger, H. Reservoir computing approaches to recurrent neural network training. *Comput. Sci. Rev.* **3(3)**, 127-149 (2009).

[7] Verstraeten, D., Schrauwen, B., d'Haene, M., & Stroobandt, D. An experimental unification of reservoir computing methods. *Neural Netw.* **20(3)**, 391-403 (2007).

[8] Tanaka, H., et al. A molecular neuromorphic network device consisting of single-walled carbon nanotubes complexed with polyoxometalate. *Nat. Commun.* **9(1)**, 1-7 (2018).

[9] Chen, T., et al. Classification with a disordered dopant-atom network in silicon. *Nature* **577(7790)**, 341-345 (2020).

[10] Tanaka, G. et al. Recent advances in physical reservoir computing: A review. *Neural Netw.* **115**, 100-123 (2019).

[11] Kan, S. K. et al. Simple reservoir computing capitalizing on the nonlinear response of materials: theory and physical implementations. *Phys. Rev. Appl.* **15**, 024030 (2021).

[12] Nakajima, K. et al. Information processing via physical soft body. *Sci. Rep.* **5(1)**, 1 (2015).

[13] Torrejon, J. et al. Neuromorphic computing with nanoscale spintronic oscillators. *Nature* **547(7664)**, 428-431 (2017).

[14] Martinenghi, R., Rybalko, S., Jacquot, M., Chembo, Y. K., & Larger, L. Photonic nonlinear transient computing with multiple-delay wavelength dynamics. *Phys Rev. Lett.* **108(24)**, 244101 (2012).

[15] Demis, E. C. et al. Atomic switch networks—nanoarchitectonic design of a complex system for natural computing. *Nanotechnology* ***26*****(20)**, 204003 (2015).

[16] Ohno, T. et al. Short-term plasticity and long-term potentiation mimicked in single inorganic synapses. *Nat. Mater.* **10(8)**, 591-595 (2011).

[17] Terabe, K., Hasegawa, T., Nakayama, T., & Aono, M. Quantized conductance atomic switch. *Nature* **433(7021)**, 47-50 (2005).

[18] Eigler, D. M., Lutz, C. P., & Rudge, W. E. An atomic switch realized with the scanning tunnelling microscope. *Nature* **352(6336)**, 600-603 (1991).

[19] Demis, E. C. et al. Nanoarchitectonic atomic switch networks for unconventional computing. *Jpn. J. Appl. Phys.* **55(11)**, 1102B2 (2016).

[20] Mi, W. et al. Thermoelectric transport of Se-rich Ag2Se in normal phases and phase transitions. *Appl. Phys. Letters* **104(13)**, 133903 (2014).

[21] Ferhat, M., & Nagao, J. Thermoelectric and transport properties of β-Ag 2 Se compounds. *J. Appl. Phys.* **88(2)**, 813-816 (2000).

[22] Xiao, C. et al. Superionic phase transition in silver chalcogenide nanocrystals realizing optimized thermoelectric performance. *J. Am. Chem. Soc.* **134(9)**, 4287-4293 (2012).

[23] Schoen, D. T., Xie, C., & Cui, Y. Electrical switching and phase transformation in silver selenide nanowires. *J. Am. Chem. Soc.* **129(14)**, 4116-4117 (2007).

[24] Zhang, J., Fu, Q., Cui, Z., & Xue, Y. Size-dependent melting thermodynamic properties of selenium nanowires in theory and experiment. *CrystEngComm* **21(3)**, 430-438 (2019).

[25] Xia, Y. et al. One‐dimensional nanostructures: synthesis, characterization, and applications. *Adv. Mater.* **15(5)**, 353-389 (2003).

[26] Gates, B., Mayers, B., Grossman, A., & Xia, Y. A sonochemical approach to the synthesis of crystalline selenium nanowires in solutions and on solid supports. *Adv. Mater.* **14(23)**, 1749-1752 (2002).

[27] Scharnhorst, K. S. et al. Atomic switch networks as complex adaptive systems. *Jpn. J. Appl. Phys.* **57(3S2)**, 03ED02 (2018).

[28] Dutoit, X. et al. Pruning and regularization in reservoir computing. *Neurocomputing* **72(7-9)**, 1534-1546 (2009).

[29] Jackson, Z. et al. Jakobovski/free-spoken-digit-dataset: v1. 0.8 (2018).

[30] Tang, Y., Zhang, Y. Q., Chawla, N. V., & Krasser, S. SVMs modeling for highly imbalanced classification. *IEEE Trans. Syst. Man. Cybern. B Cybern.* **39(1)**, 281-288 (2008).

[31] Sellam, V., & Jagadeesan, J. Classification of normal and pathological voice using SVM and RBFNN. *J. Signal Inf. Process. 2014* (2014).

[32] Cawley, G. C., & Talbot, N. L. On over-fitting in model selection and subsequent selection bias in performance evaluation. *J. Mach. Learn. Res.* **11**, 2079-2107 (2010).

Figures

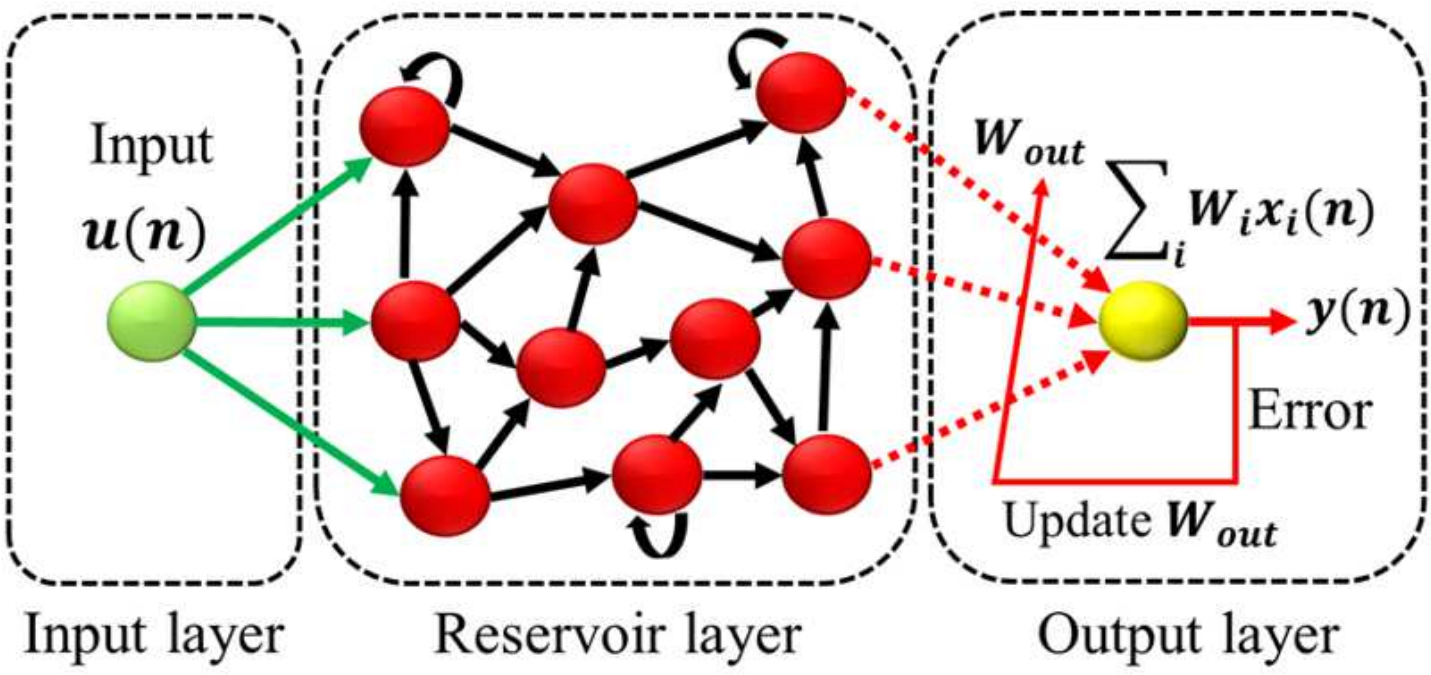

Figure 1

Reservoir computing (RC). An RC system is composed of three layers: input, reservoir, and output. The calculated wavefunction is a linear combination of output signals, weighted through learning to ensure the best approximation to a target waveform, y(n).

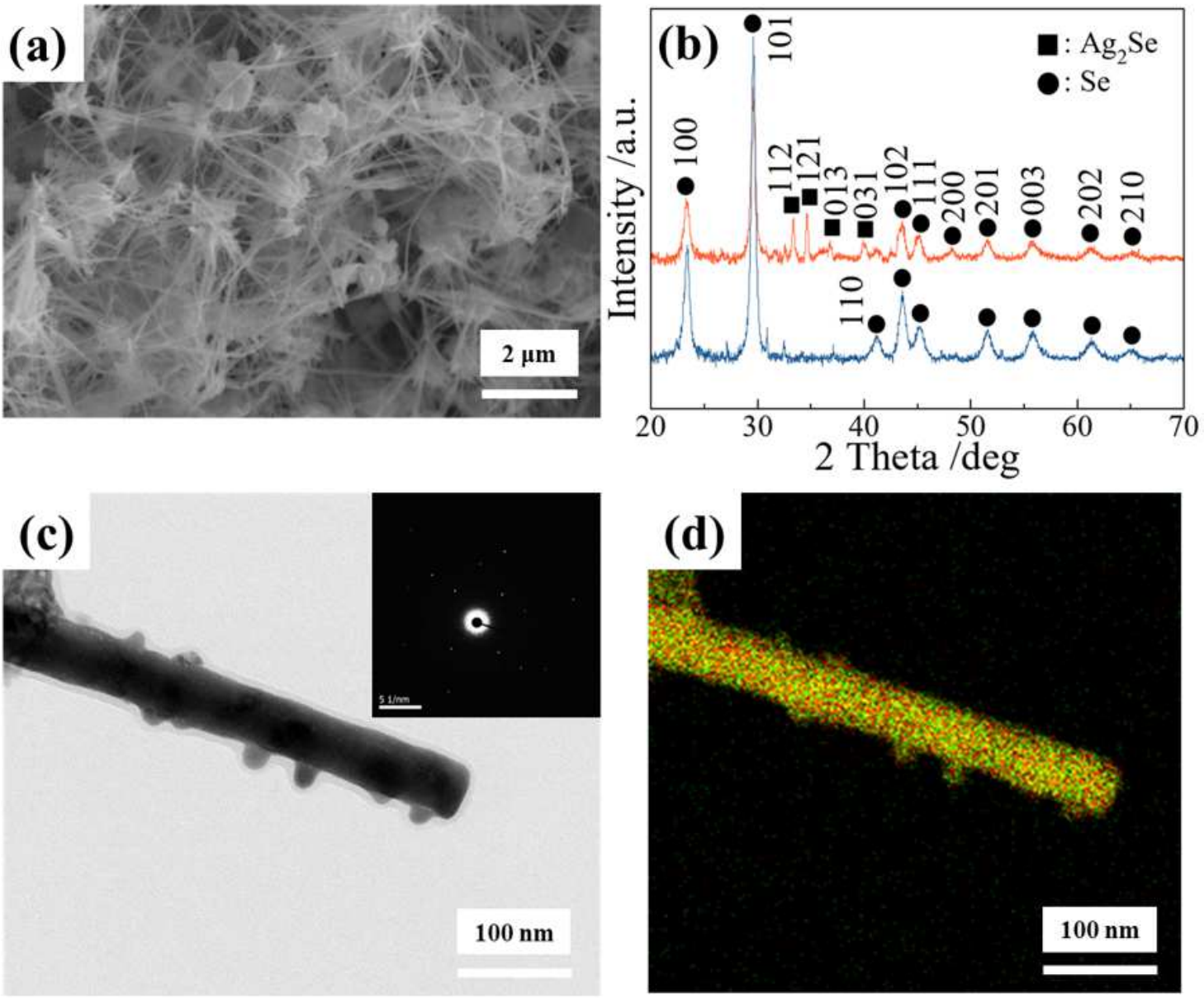

Figure 2

Structural characterization of Ag2Se. a, SEM image and b, XRD results of synthesized Ag2Se nanowires after submerging in a AgNO3 solution. The blue and orange curves represent the nanowires before and after reaction in the AgNO3 solution, respectively. c, STEM image of synthesized Ag2Se nanowire. Inset: SAED pattern of Ag2Se indicating single crystallinity. d, EDS results showing stoichiometric distribution of Ag and Se in the Ag2Se nanowire. Red and green dots indicate the positions of Ag and Se, respectively.

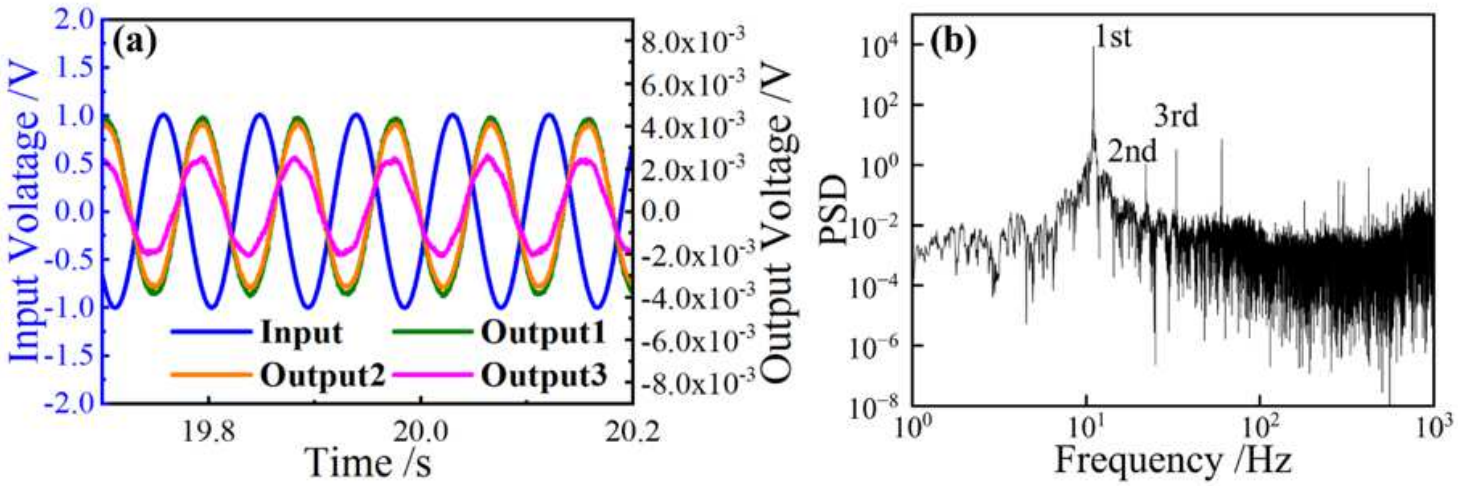

Figure 3

Electronic properties of Ag2Se nanowire device. a, V-t curves and b, PSD diagram for a device responding to an input signal. Four probes were used for the V-t measurements where the input signal was a sinusoidal voltage (amplitude: ± 1 V, frequency: 11 Hz) and there were three output signals. The blue curve represents the input signal. The output signals were obtained from a random network device made from Ag2Se nanowires.

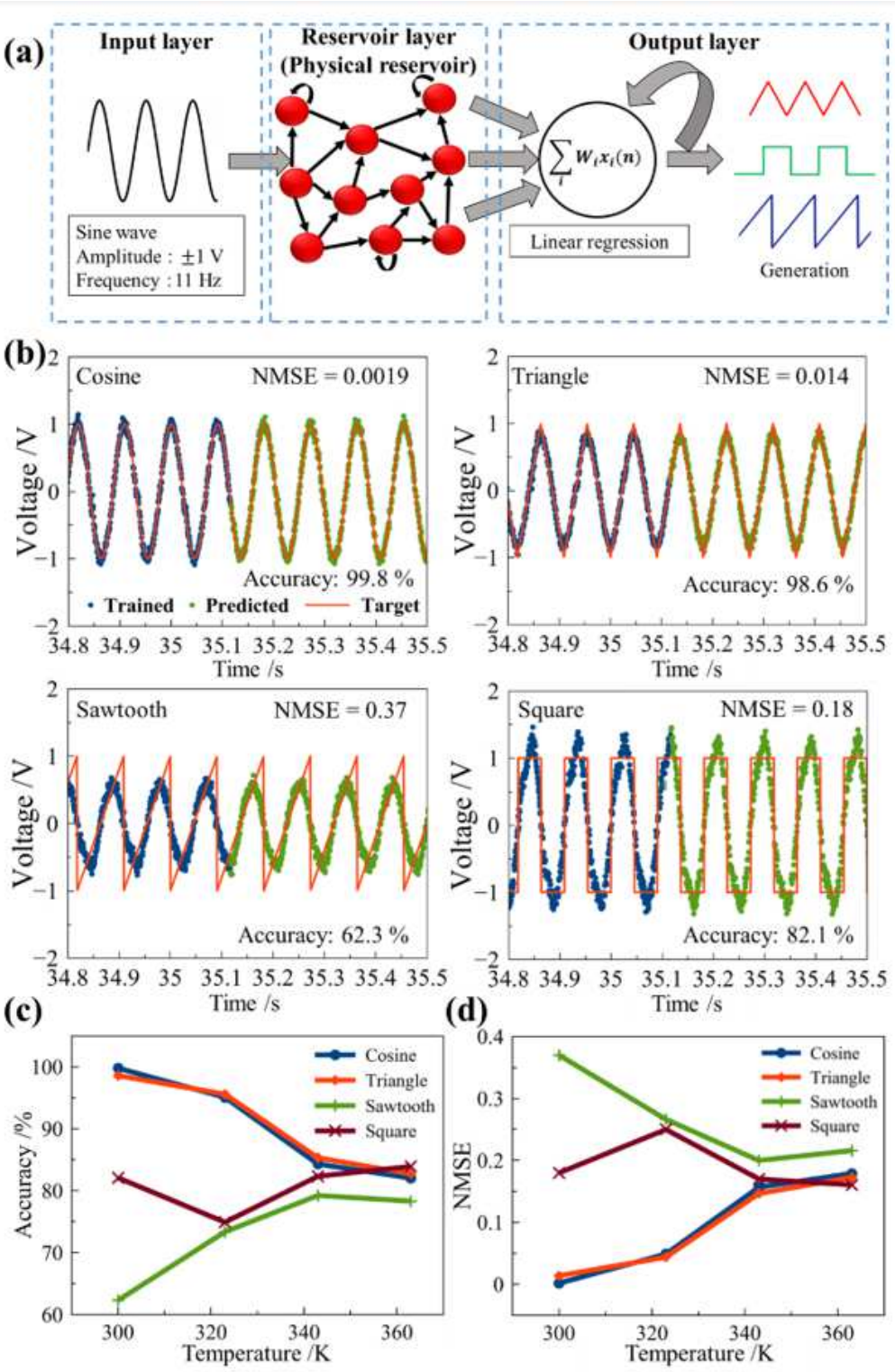

Figure 4

Results of waveform generation task. a, Procedure for waveform-generation task. The input was a sinusoidal wave (amplitude: ± 1 V, frequency: 11 Hz) in air. b, Results of waveform generation tasks at room temperature. Target waves were cosine, triangle, sawtooth, and square waves shown at top left, top right, bottom left, and bottom right, respectively. NMSE is an abbreviation for “normalized mean square error.” c,d, Accuracy and NMSE of specific tasks at different temperatures, respectively.

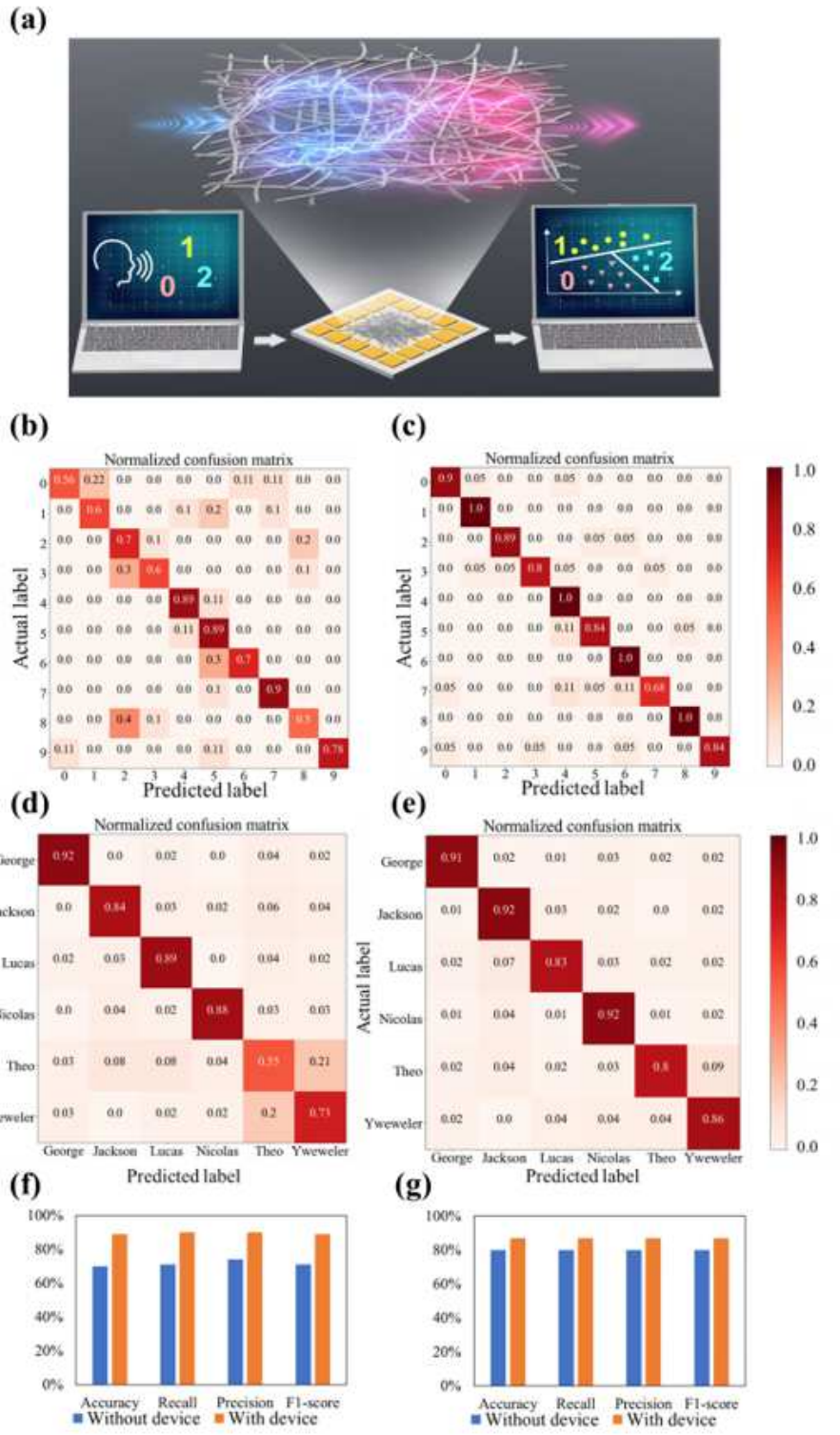

Figure 5

Classification results for ten numbers and six speakers. a, Schamatic of voice classification procedure. FSDD was utilized as the voice dataset. Six speakers (George, Jackson, Nicolas, Theo, Yweweler, and Lucas) and ten numbers from zero to nine were classified. The voice data was subjected to FFT preprocessing and was fed into to the Ag2Se device as an analog signal. There was one input and two outputs, and the input was an analog-converted signal from 0 to 9. Outputs were labeled and used for

model construction and the determination of test performance. Confusion matrices b, without and c, with the Ag2Se reservoir device of classifying ten numbers from zero to nine spoken by Jackson, respectively. d,e, Confusion matrices classifying six speakers d without and e with the Ag2Se reservoir device. f,g, Classification scores with and without the Ag2Se reservoir device for f ten numbers and g six speakers.

Supplementary Files

This is a list of supplementary files associated with this preprint. Click to download.

- ForEngEdiAg2Senanowiernetworksubmissionver2nomodificationhistorySI.docx